Australasian Physical & Engineering Sciences in Medicine (2019) 42:819–826
https://doi.org/10.1007/s13246-019-00762-5

TECHNICAL PAPER

Improving automatic contrast agent extraction system using monochromatic CT number

Daisuke Kawahara[1] · Shuichi Ozawa[2,3] · Kazushi Yokomachi[1] · Toru Higaki[4] · Chikako Fujioka[1] · Masayoshi Mori[1] · Yasushi Nagata[2,3]

Received: 17 January 2019 / Accepted: 8 May 2019 / Published online: 20 May 2019

Abstract

In a previous study, a phantom study of a contrast agent extraction system with computed tomography (CT) number and raw-data-based electron density (ED) was described. The current study improved this system with monochromatic CT (mCT) number and evaluated an anthropomorphic phantom for delineation of the contrast-enhanced region. Dual-energy CT images were scanned with a tissue-equivalent phantom and an anthropomorphic phantom with an iodinated contrast agent (1–130 mg/mL). The 40, 70, and 130 keV mCT images were reconstructed with 80 and 135 kV CT images. The contrast agent was separated from other materials using the gradient of the mCT number (GmCT) and the threshold mCT numbers. The system was analyzed using in-house software with Python. The evaluation of the accuracy for the contrast agent extraction was performed by measuring the ratio of the volume (ROV). The mCT number of the contrast agent and bone materials, liver, and muscle in the tissue-equivalent phantom was obviously greater than −78 HU. The deviation of the mCT numbers between bone materials in tissue-equivalent phantom and the contrast agent were larger than 8 HU. The GmCT was within 4.0 in the tissue-equivalent phantom and more than 6.0 in the contrast agent. The ROV was 0.97–1.00 at more than 1 mg/mL contrast agent. Improved the contrast agent extraction system could be used for a patient's CT image. It could extract the iodinated tumor or lesion automatically. The contrast agent extraction system was improved by the mCT number. It is expected to only extract the contrast-enhanced region automatically.

Keywords Monochromatic CT number · Dual-energy CT · Contrast agent

Introduction

Novel innovations in computed tomography (CT) technology have made dual-energy CT (DECT) clinically applicable for the automatic characterization of kidney stone classifications, gout detection, and automatic bone removal [1–3]. To improve tissue characterization, DECT provides various information, such as the electron density (ED), effective atomic number, and monochromatic CT (mCT) number based on exploiting the difference of the tissues that depend on the attenuation [4–6]. Alvarez et al. introduced the virtual mCT, which allowed the reconstruction at a mono-energy level within 40–140 keV or more [7]. It could reduce beam hardening artifacts such as dense materials, improve iodine contrast for CT angiography, and achieve better soft-tissue contrast for radiation diagnosis and radiotherapy treatment planning [8–11].

Contrast agent unenhanced and enhanced CT has been used for many clinical studies [12, 13]. In treatment

This work was presented in part at the 60th Annual Meeting & Exhibition of The American Association of Physicists in Medicine (AAPM), 2017.

✉ Daisuke Kawahara
daika99@hiroshima-u.ac.jp

[1] Radiation Therapy Section, Division of Clinical Support, Hiroshima University Hospital, 1-2-3 Kasumi, Minami-ku, Hiroshima City 734-8551, Japan

[2] Department of Radiation Oncology, Institute of Biomedical & Health Sciences, Hiroshima University, Hiroshima City 734-8551, Japan

[3] Hiroshima High-Precision Radiotherapy Cancer Center, Hiroshima City 732-0057, Japan

[4] Departments of Diagnostic Radiology and Radiology, Hiroshima University, Hiroshima City 732-0057, Japan

planning, a contrast agent is used to delineate the normal and the targeted structures. Usually, a water-soluble contrast agent is washed out after scanned CT. Lipiodol, that is an oily contrast agent and a mixed anticancer agent, can be used for liver cancer. Our previous study showed the dose enhancement caused by Lipiodol for liver cancer radiation therapy [14]. We showed that the material assignment of the contrast agent cannot be performed on a recent commercial treatment planning device. Thus, it is necessary to extract the targeted region. Previously, we reported a contrast agent extraction system using the CT number and raw-data-based ED [15]. We evaluated with a simplified acryl phantom. The lower limit of the concentration of the contrast agent extraction was within 2 mg/mL.

Our objectives of the present study were to evaluate the contrast agent extraction system with the anthropomorphic phantom and to improve the accuracy of the contrast agent extraction with new contrast agent extraction system with the mCT number.

Materials and methods

Two phantoms were used in the current study, as shown in Fig. 1a. One was a tissue-equivalent phantom model 062 M (Computerized Imaging Reference Systems, Inc., Norfolk, VA, USA). This phantom contained 10 different inserts (muscle, liver, water, lung inhale, lung exhale, adipose, breast, and bone materials. The other phantom was a multipurpose chest phantom (LUNGMAN N1; Kyoto Kagaku) that the contrast agent (Omnipaque 300, GE Healthcare, Princeton, USA) was inserted, as shown in Fig. 1b. Sixteen different concentrations of iodinated contrast agent (1–130 mg/mL) were positioned around the center of the LUNGMAN phantom. DECT scans were performed with

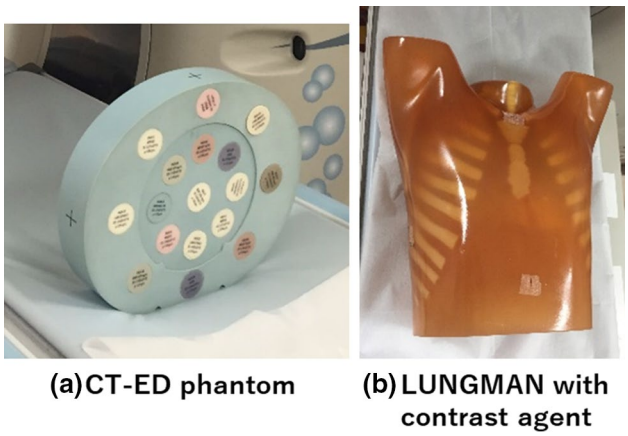

Fig. 1 **a** Tissue-equivalent phantom model 062 M and **b** LUNGMAN phantom with different concentrations of contrast agent

a 320-detector CT scanner (Toshiba Medical Systems Corporation, Japan). The tube voltages of DECT scan mode is set as 80/135 kV. The tube currents were used 800 and 200 mA for 80 kV and 135 kV, respectively. The other scan parameters were 1.0 s for rotation time and 400 mm for the field of view.

mCT number measurement

The middle axial slice of DECT images was analyzed with ImageJ software package (National Institutes of Health, USA). DECT could generate mCT images with sinogram of high and low tube voltage. The mCT number was calculated with a linear attenuation coefficient. The linear attenuation coefficient μ of material could be expressed in photoelectric absorption and Compton scattering (excluding K-edge effects) as

$$\mu(E) = a_p f_p(E) + a_c f_c(E), \tag{1}$$

where a_p and f_p are material constants and constants that depend on the E that is photon energy in photoelectric absorption. The a_c and f_c are material constants and constants that depend on the E in Compton scattering, respectively [5]. This equation can be simplified as

$$\mu(E) = f\left(\rho_e, Z_{eff}, E\right) + f\left(\rho_e\right), \tag{2}$$

where ρ_e is the rED number, and Z_{eff} is the effective atomic number. Moreover, in DECT processing, the attenuation coefficient is modified as

$$\mu(E) = \mu_1(E)m_1 + \mu_2(E)m_2, \tag{3}$$

where μ_1(E) and μ_2(E) are the mass attenuations of the basis materials a and b. The coefficients m_1 and m_2 are constants that depend on two E values of photoelectric absorption and Compton scattering, respectively. The mCT numbers were derived from the mass attenuation coefficient as follows.

$$CT\#_i(\mathrm{E}) = \left[\frac{\mu(E) - \mu(E)_{water}}{\mu(E)_{water-\mu(E)_{air}}}\right] \times 1000 \tag{6}$$

where μ(E), $\mu(\mathrm{E})_{water}$ and $\mu(\mathrm{E})_{air}$ are the mass attenuation of each materials, water, and air The mCT images were obtained at 40–130 keV in increments of 10 keV.

The contrast agent extraction method

The contrast agent extraction system was built with Python 2.7. As shown in Fig. 2, this system contains several processes. The mCT images at 40, 70 and 130 keV were input and the threshold of the mCT number was used in Step 1 to eliminate the lower mCT numbers such as lung inhale, lung exhale, breast, and adipose. The detection of

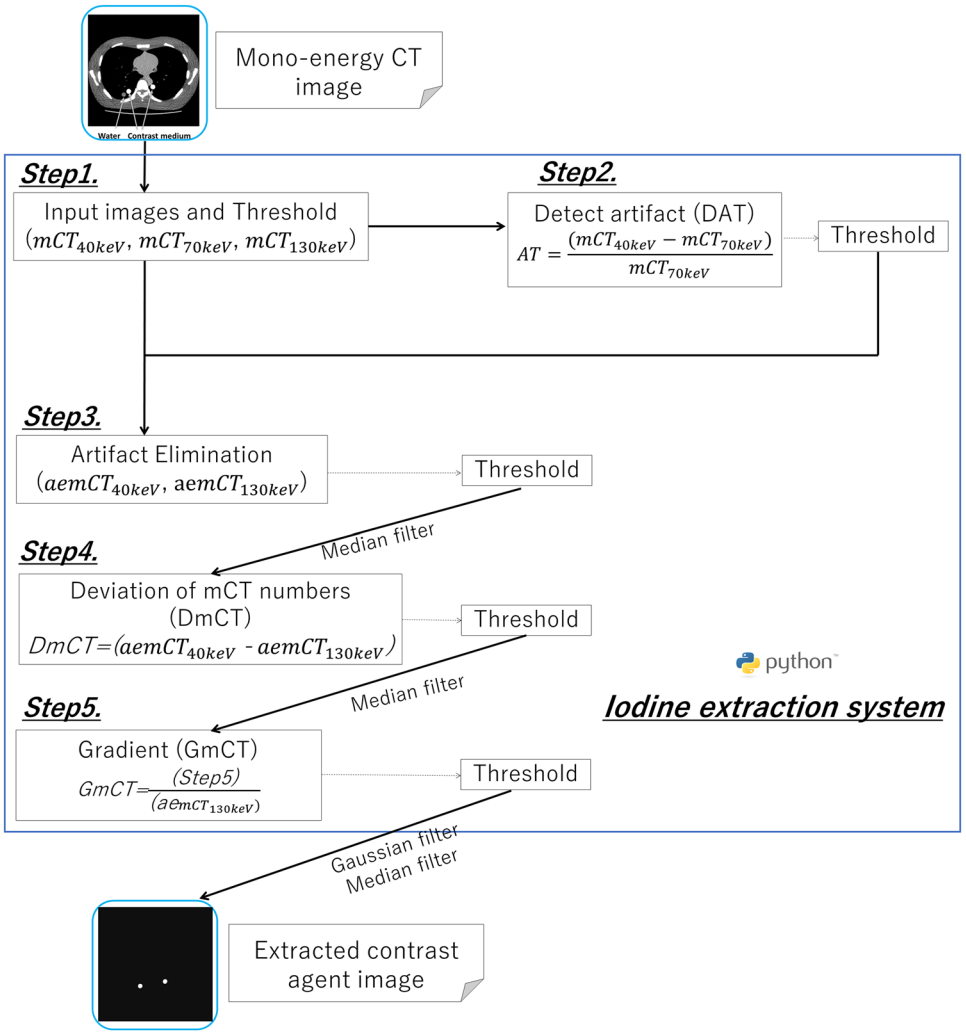

Fig. 2 The process of the automatic contrast agent extraction system with Python 2.7. The input was used for mCT image at 40, 70 and 130 keV. For Step 1, the lower mCT numbers were eliminated. The detection and elimination of beam-hardening artifacts were performed in Steps 2 and 3. For Step 4 and 5, the contrast agent was extracted by using the difference of the attenuation that depends on the materials and energies. At each step, three-dimensional Gaussian filtering or median filtering were used for denoising each image

beam-hardening artifact (DAT) was performed in Steps 2 because there were some beam-hardening artifacts (ATs) at low-energy (40 keV). Here, the mCT image at 70 keV was used, because the AT was smaller than that at 40 keV and the differences between the theoretical and measured mCT numbers in the contrast agent and the tissue-equivalent phantom were small, which was shown in the past study [16]. Using the DAT images, the region of ATs was eliminated in mCT images at 40 and 130 keV in Steps 3. The AT eliminated images were defined as artifact eliminated mCT (aemCT) images. In Step 4, the deviation of the mCT numbers (DmCT) between high energy (130 keV) and low energy (40 keV) were calculated. Finally, the gradients of the mCT (GmCT) numbers were calculated from the mCT images at 40 and 130 keV in Step 5. For Step 4 and 5, the contrast agent was extracted by using the difference of the attenuation that depends on the materials and energies. At each step, three-dimensional Gaussian filtering and median filtering were used for denoising each image. After extraction of the contrast agent, the accuracy was evaluated by measuring the ratio of the volume (ROV) between the CT image and the contrast agent-extracted image. The ROV was calculated by

$$\mathrm{ROV} = \frac{V_{\mathrm{ext}}}{V_{\mathrm{ref}}}$$

where V_{ext} and V_{ref} were extracted and reference the volume of the contrast agent, respectively. Here, V_{ext} was the region of the extracted contrast using the contrast agent extraction system. The V_{ext} was measured using Image J. V_{ref} was reference volume that included the contrast agent, that was 40 cc.

Results

Measured mCT numbers

The mCT numbers and DmCT in the CT-ED phantom, as shown in Fig. 3. The mean-2SD (standard deviation) mCT

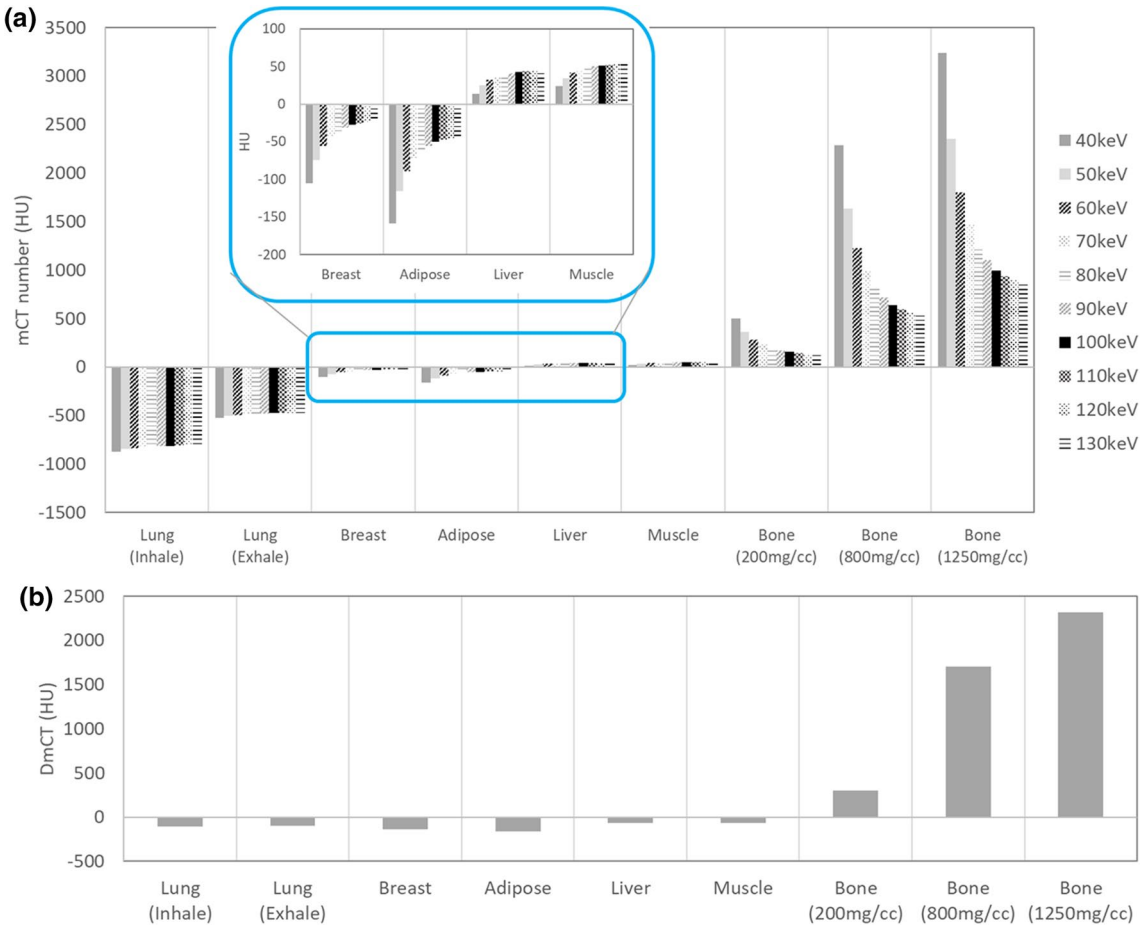

Fig. 3 **a** Measured mCT numbers in the tissue-equivalent phantom and **b** DmCT numbers in the tissue-equivalent phantom

numbers of the lung inhale, lung exhale, breast, and adipose were < -211 HU at 40, 70, and 130 keV energies. However, the mean-2SD mCT numbers of the muscle, liver, bone materials were larger than -55 HU at 40, 70, and 130 keV energies. The mean-2SD DmCT numbers of the bone materials were larger than 301 HU.

Figure 4 shows the mCT numbers and DmCT in the LUNGMAN phantom in which the contrast agent syringe was inserted. The mean-2SD mCT numbers at all energies and mean-2SD DmCTs of the contrast agent at 1–130 mg/ml were larger than -73 and 8 HU, respectively. The mCT numbers with lower energy were larger for the contrast agent. There is a strong correlation ($r > 0.99$) between DmCT and the concentration of the contrast agent.

Figure 5 shows the GmCTs in the tissue-equivalent phantom and the LUNGMAN phantom. The GmCT values of the lung (inhale), lung (exhale), liver, and muscle in the tissue-equivalent phantom were smaller than 0 HU. Although the GmCTs of the breast, adipose, trabecular bone, dense bone, and higher density bone were more than 0 HU, these were smaller than 3.7. However, the GmCTs in the contrast agent at all concentrations were more than 6.0. The GmCTs in the contrast agent at 1–130 mg/ml were larger than that in the tissue-equivalent materials.

Contrast agent extraction

As indicated in Section A, the mean-2SD mCT numbers of the contrast agent at 1–130 mg/ml were greater than -73 HU at 40, 70, and 130 keV energies, and the DmCT was also greater than 8 HU at 40, 70, and 130 keV energies. Therefore, the threshold values of the mCT and DmCT numbers were -100 HU and 0 HU at Steps 1 and 4. For Step2 of DAT, the maximum AT value at a concentration of 130 mg/ml was 2.1, and the beam-hardening AT at more than 2.1 in AT image was eliminated (Steps 3). From the result of Fig. 5, the GmCT was within 4.0 with the tissue-equivalent phantom and over 6.0 with the contrast agent at 1–130 mg/ml. Thus, the threshold value used in Step 5 was 6.0. The concentration of the contrast agent was assigned using the correlation between the contrast agent concentration and the mCT number, as shown in Fig. 4a. Figure 6 shows the mCT

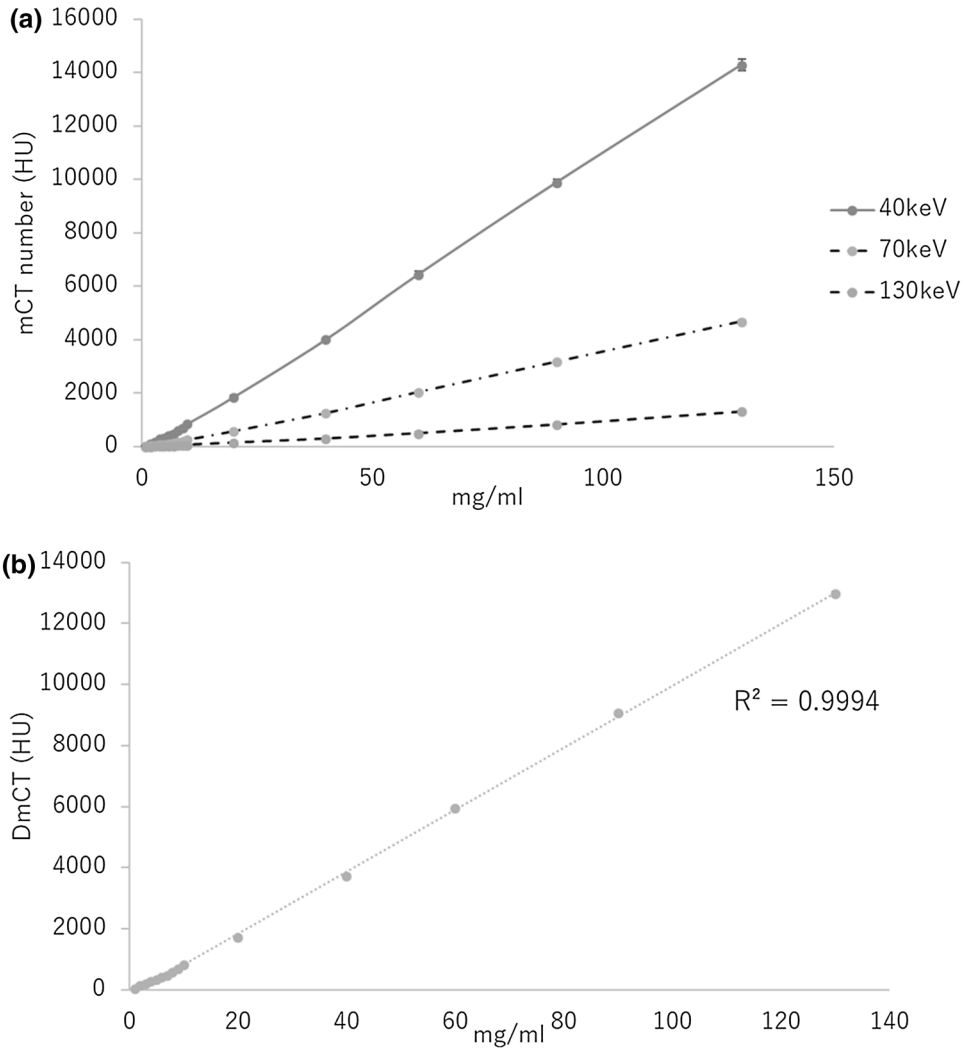

Fig. 4 **a** Measured mCT numbers in the LUNGMAN phantom that the syringe filled with contrast agent at 1–130 mg/ml and **b** DmCT numbers in the LUNGMAN phantom that the syringe filled with contrast agent at 1–130 mg/ml

image at 70 keV and the iodine density image and the contrast agent extracted images from the LUNGMAN phantom with contrast agent that the syringe filled with a contrast agent at 10 and 20 mg/m. In the iodine density image, the contrast agent is highlighted, but on the other hand the other materials are not eliminated. For the contrast agent extracted image, only the contrast enhanced region was extracted. The accuracy of the contrast agent is shown in Table 1. The ratio of the measurement to the actual diameter in the ROV was 0.97–1.00 with the contrast agent at 1–130 mg/ml.

Discussion

The mCT numbers for the contrast agent and the bone materials were higher at lower energies. The DmCT for the contrast agent and the bone materials was also larger than 0 HU. For high-density materials such as the contrast agent and the bone materials, the photoelectric effect is dominant interaction with low-energy radiation. The GmCT was more than 6.0 in the contrast agent at 1–130 mg/ml, which was significantly larger than tissue equivalent inserts that were within 3.7. The attenuation of the iodine was larger than those of tissue-equivalent inserts; thus, the difference of the mCT number between the contrast agent and hose of tissue-equivalent inserts was larger according to monochromatic energies. Therefore, the DmCT and the GmCT are useful for the extraction of the contrast agent. However, the beam-hardening AT was a serious problem for mCT images. Yu et al. reported that beam-hardening ATs were contained in lower monochromatic energy images [17]. This evaluation shows that the synthesized virtual monochromatic images generated from the current DECT devices are not accurately monochromatic. The beam-hardening AT of low-energy images was reduced by using the DAT in Step 2 and 3.

Material decomposition with DECT data can create an iodine density image that highlights the contrast agent and contrast unenhanced image [18]. The contrast-enhanced and -unenhanced images could help radiation diagnosis. Although, Lasta et al. showed that the iodine map provided

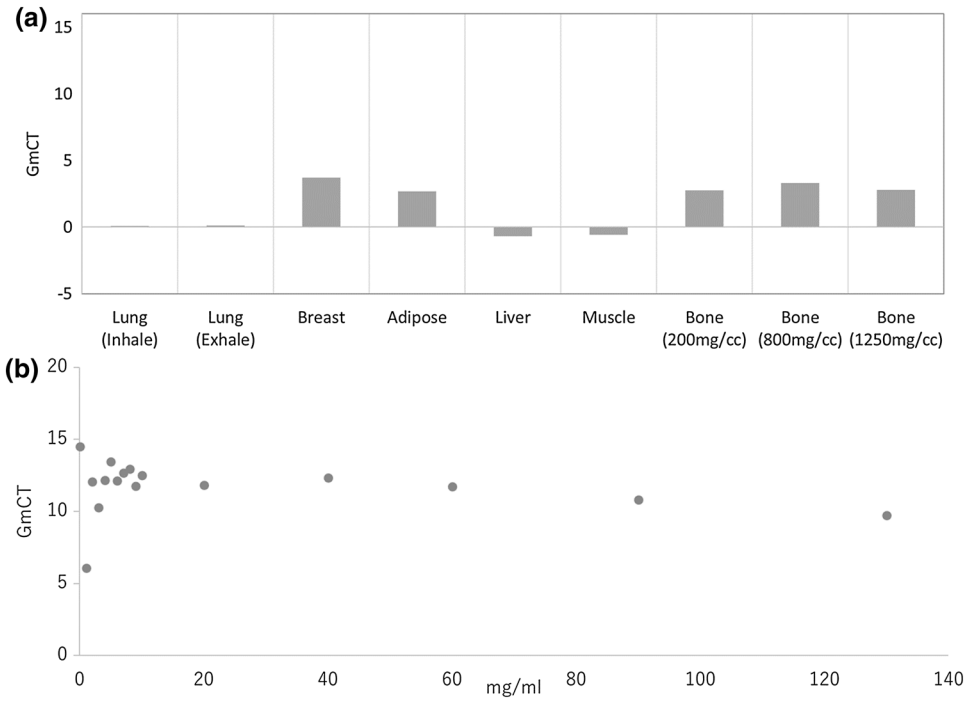

Fig. 5 **a** GmCT numbers in the tissue-equivalent phantom, and **b** GmCT numbers in the LUNGMAN phantom that the syringe filled with contrast agent at 1–130 mg/ml

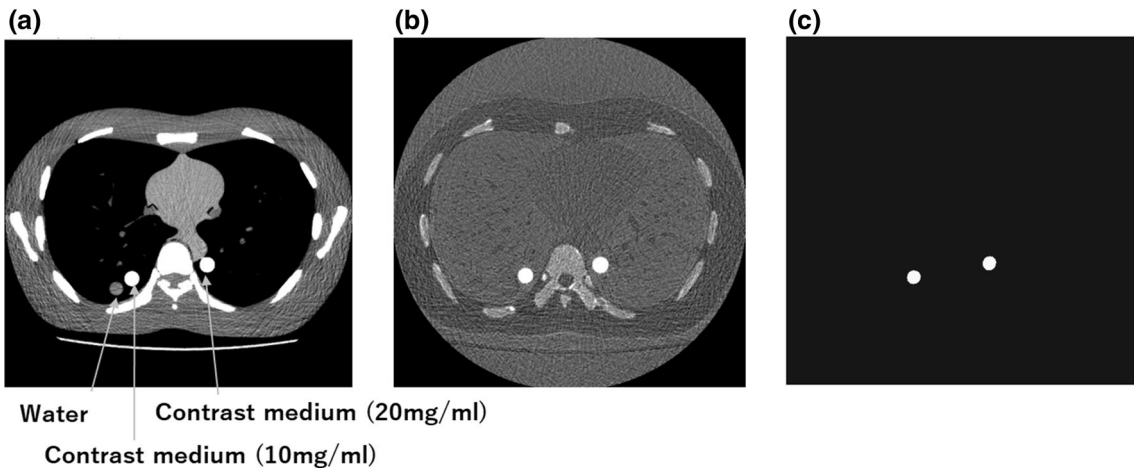

Fig. 6 **a** mCT image at 70 keV, **b** reconstructed iodine density image and **c** contrast agent extracted images in the LUNGMAN phantom that the syringe filled with contrast agent at 10 and 20 mg/ml

Table 1 Limit concentration accuracy of the contrast agent

mg/ml	1	2	3	4	5	6	7	8	9	10	20	40	60	90	130
ROV	0.98	0.98	0.98	0.98	0.99	0.99	0.99	0.98	0.99	0.99	1.00	0.99	1.00	0.99	1.00

a good visualization of pancreatic cancer, the iodine density image cannot eliminate the bone materials [19]. Our contrast extraction system could fully extract only the region containing the contrast agent.

The interobserver variability for the target delineation could be a serious problem for radiation diagnosis and treatment planning [20, 21]. The previous system using CT numbers and rED could extract the contrast agent at more than 2 mg/ml with a simple acryl phantom inserted in the contrast agent. In the current study, the contrast agent extraction system using the mCT numbers was created and evaluated with the anthropomorphic phantom. The lower limit

of the concentration of the contrast agent extraction system was improved at more than 1 mg/ml. The contrast scale in the mCT numbers was determined for air and water. The contrast scales in the electron density and CT number were smaller than the mCT numbers. Thus, the mCT numbers are useful for contrast agent extraction at low concentration. From above, this improved contrast agent extraction system could be useful for automatic extraction of a contrast-enhanced tumor or other diseases in radiation diagnosis and radiation treatment planning.

DECT reconstruction techniques would be different according to vendors. For example, GE Discovery 750HD and Revolution (GE Healthcare, Milwaukee, WI) can combine the monoenergetic image reconstruction with a metal AT reduction software (MARS). According to the vendor, the MARS algorithm is designed to correct for extreme beam-hardening ATs under severe low-signal conditions owing to photon starvation. The accuracy of the contrast agent extraction by beam-hardening ATs should be investigated with any other vendor's DECT system.

Conclusion

It is possible to detect and eliminate the beam hardening artifacts and extract the contrast agent could be performed by using mCT images at low and high energies. The contrast agent extraction method could be used at contrast agent concentration 1 mg/mL or more, which was improved by comparing it with a previously developed system. The method developed in this study would extract the contrast-enhanced tumor or lesion within the human body automatically.

Compliance with ethical standards

Conflict of interest The authors declare that they have no conflict of interest.

Informed consent For this type of study formal consent is not required.

Research involving human participants and/or animals The authors did not use the human or other animals. This study only used the phantom.

References

1. Kaemmerer N, Brand M, Hammon M, May M, Wuest W, Krauss B et al (2016) Dual-energy computed tomography angiography of the head and neck with single-source computed tomography: a new technical (split filter) approach for bone removal. Invest Radiol 51(10):618–623
2. Primak AN, Fletcher JG, Vrtiska TJ, Dzyubak OP, Lieske JC, Jackson ME et al (2007) Noninvasive differentiation of uric acid versus nonuric acid kidney stones using dual-energy CT. Acad Radiol 14:1441–1447
3. Michalak G, Grimes J et al (2016) Improved CT number stability across patient size using dual-energy CT virtual monoenergetic imaging. Med Phys 43(1):513
4. Petersilka M, Bruder H, Krauss B et al (2008) Technical principles of dual source CT. Eur J Radiol 68:362–368
5. Meier A, Wurnig M, Desbiolles L, Leschka S et al (2015) Advanced virtual monoenergetic images: improving the contrast of dual-energy CT pulmonary angiography. Clin Radiol 70(11):1244–1251
6. Kawahara D, Ozawa S, Yokomachi K (2018) Accuracy of the raw-data-based effective atomic numbers and monochromatic CT numbers for contrast agent with a dual-energy CT technique. Br J Radiol 91(1082):20170524
7. Alvarez RE, Macovski A (1976) Energy-selective reconstructions in X-ray computerized tomography. Phys Med Biol 21(5):733–744
8. Bamberg F, Dierks A, Nikolaou K et al (2011) Metal artifact reduction by dual energy computed tomography using monoenergetic extrapolation. Eur Radiol 21:1424–1429
9. Yamada S, Ueguchi T, Shimosegawa E et al (2015) Feasibility of improved attenuation correction for SPECT reconstruction in the presence of dense materials using dual-energy virtual monochromatic CT: a phantom study. Open J Med Imaging 5:183–193
10. Leng S, Yu L, Fletcher JG et al (2015) Maximizing iodine contrast-to-noise ratios in abdominal CT imaging through use of energy domain noise reduction and virtual monoenergetic dual-energy CT. Radiology 276:562–570
11. Agrawal MD, Oliveira GR, Kalva SP et al (2016) Prospective comparison of reduced-iodine-dose virtual monochromatic imaging dataset from dualenergy CT angiography with standard-iodine-dose single-energy CT angiography for abdominal aortic aneurysm. AJR Am J Roentgenol 207:W125–W132
12. Kang M-J, Park CM, Lee C-H, Goo JM, Lee HJ (2010) Dual-energy CT: clinical applications in various pulmonary diseases. Radiographics 30(3):685–698
13. Yamada S, Ueguchi T, Ogata T (2014) Radiotherapy treatment planning with contrast-enhanced computed tomography: feasibility of dual-energy virtual unenhanced imaging for improved dose calculations. Radiat Oncol 29(9):168
14. Kawahara D, Oawa S et al (2017) Dosimetric impact of lipiodol in stereotactic body radiation therapy on liver after trans-arterial chemoembolization. Med Phys 44(1):342–348
15. Kawahara D, Ozawa S, Tanaka S et al (2018) Automatic contrast agent extraction system using electron density data with dual-energy CT. Br J Radiol 9:20180396
16. Kawahara D, Ozawa S, Yokomachi K et al (2018) Accuracy of the raw-data-based effective atomic numbers and monochromatic CT numbers for contrast agent with a dual-energy CT technique. Br J Radiol 91(1082):20170524
17. Yu L, Leng S, McCollough CH (2012) Dual-energy CT-based monochromatic imaging. AJR Am J Roentgenol 199(5 Suppl):S9–S15
18. Coursey CA, Nelson RC, Boll DT, Paulson EK, Ho LM, Neville AM, Marin D, Gupta RT, Schindera ST (2010) Dual-energy multidetector CT: how does it work, what can it tell us, and when can we use it in abdominopelvic imaging? Radiographics 30:1037–1055
19. Lastra T, Mule S, Millet I et al (2016) Applications of dual energy computed tomography in abdominal imaging. Diagn Interv Imaging 97(6):593–603
20. Sverzellati N, Molinari F, Pirronti T (2007) New insights on COPD imaging via CT and MRI. Int J Chron Obstruct Pulmon Dis. 2(3):301–312

21. Gkika E, Tanadini-Lang S, Kirste S et al (2017) Interobserver variability in target volume delineation of hepatocellular carcinoma: an analysis of the working group "stereotactic radiotherapy" of the German society for radiation oncology (DEGRO). Strahlenther Onkol 193(10):823–830